

This is the author's version of the work.

It is posted here by permission of the AAAS for personal use, not for redistribution.

The definitive version was published in *Science Signaling* on Vol.7, Issue 343, 16 September 2014, DOI: 10.1126/scisignal.2005522.

The final version published on the Science Web site:

<http://stke.sciencemag.org/content/7/343/ra88.abstract>

## Protective effect of the long pentraxin PTX3 against histone-mediated endothelial cell cytotoxicity in sepsis

Kenji Daigo,<sup>1\*</sup> Makoto Nakakido,<sup>2†</sup> Riuko Ohashi,<sup>3,4</sup> Rie Fukuda,<sup>1</sup> Koichi Matsubara,<sup>3</sup> Takashi Minami,<sup>5</sup> Naotaka Yamaguchi,<sup>6</sup> Kenji Inoue,<sup>7</sup> Shuying Jiang,<sup>3,8,9</sup> Makoto Naito,<sup>3</sup> Kouhei Tsumoto,<sup>2</sup> Takao Hamakubo<sup>1‡</sup>

<sup>1</sup>Department of Quantitative Biology and Medicine, Research Center for Advanced Science and Technology, The University of Tokyo, Tokyo, Japan. <sup>2</sup>Laboratory of Medical Proteomics, Institute of Medical Science, The University of Tokyo, Tokyo, Japan. <sup>3</sup>Department of Cellular Function, Division of Cellular and Molecular Pathology, Niigata University Graduate School of Medical and Dental Sciences, Niigata, Japan. <sup>4</sup>Department of Pathology, Niigata University Medical and Dental Hospital, Niigata, Japan. <sup>5</sup>Laboratory for Vascular Biology, Research Center for Advanced Science and Technology, The University of Tokyo, Tokyo, Japan. <sup>6</sup>Department of Emergency and Critical Care Medicine, Juntendo University Nerima Hospital, Tokyo, Japan. <sup>7</sup>Department of Cardiology, Juntendo University Nerima Hospital, Tokyo, Japan. <sup>8</sup>Niigata College of Medical Technology, Niigata, Japan. <sup>9</sup>Perseus Proteomics Inc., Tokyo, Japan.

\*Current address: Humanitas Clinical and Research Center, Rozzano, Milan, Italy.

†Current address: Department of Medicine, The University of Chicago, Chicago, USA

‡Corresponding author. E-mail: hamakubo@qbm.rcast.u-tokyo.ac.jp

### Abstract

Pentraxin 3 (PTX3), a member of the long pentraxin subfamily within the family of pentraxins, is a soluble pattern-recognition molecule that functions in the innate immune system. Innate immunity affords the infected host protection against sepsis, a potentially life-threatening inflammatory response to infection. Extracellular histones are considered to be the main cause of septic death because of their cytotoxic effect on endothelial cells, which makes them a potential therapeutic target. We found that PTX3 interacted with histones to form coaggregates, which depended on polyvalent interactions and disorder in the secondary structure of PTX3. PTX3 exerted a protective effect, both *in vitro* and *in vivo*, against histone-mediated cytotoxicity towards endothelial cells. Additionally, the intraperitoneal administration of PTX3 reduced mortality in mouse models of sepsis. The N-terminal domain of PTX3, which was required for coaggregation with histones, was sufficient to protect against cytotoxicity. Our results suggest

that the host-protective effects of PTX3 in sepsis are a result of its coaggregation with histones rather than its ability to mediate pattern recognition. This long pentraxin-specific effect provides a potential basis for the treatment of sepsis directed at protecting cells from the toxic effects of extracellular histones.

## **Introduction**

Pentraxin 3 (PTX3) is one of a number of soluble pattern-recognition molecules (PRMs), which are key molecules in the innate immune system, and it belongs to the long pentraxin subfamily within the family of pentraxins (1, 2). PTX3 plays several roles in the first-line activity of the host-protective response, such as the recognition of specific pathogens and the subsequent opsonization that occurs, as well as regulation of complement and inflammation (3-5). PTX3 also plays a role in angiogenesis and female fertility (1, 6, 7). This multi-functionality of PTX3 is because of its ability to bind to many different ligands (5, 8). PTX3 has two domains: a unique N-terminal domain and a conserved C-terminal pentraxin domain, and most of its ligands bind to PTX3 in a domain-specific manner (2, 9, 10). PTX3 forms a multimeric structure through inter-molecular disulfide bonds, and it has an N-glycosylation site (5, 8).

The innate immune system plays crucial roles in the pathophysiology of sepsis, which is a major cause of death in developed countries (11). At the onset of sepsis, infectious events initiate the innate immune response through PRMs by sensing pathogen-associated molecular patterns (PAMPs) (12, 13). Subsequently, certain innate immune cells, such as macrophages, secrete pro-inflammatory mediators in response to PRMs (13, 14). An excessive immune reaction and exposure to pro-inflammatory cytokines results in a systemic inflammatory reaction (13). In

response to the innate immune reaction, neutrophils are attracted to, and activated at, the site of infection or damaged tissue. An over-accumulation of neutrophils leads to the multi-organ failure that is the direct cause of septic death, by exerting an excessive inflammatory response and concomitant cytotoxicity (14). In sepsis, the circulating concentration of PTX3 increases substantially (15-17). In addition to PAMPs, host-derived molecules, called damage-associated molecular patterns (DAMPs, also known as alarmins), also stimulate the PRM-mediated inflammatory and innate immune responses (18, 19). In the case of sterile inflammation, such as that induced by trauma, burn, ischemia, or hemorrhage, which exhibits almost the same pathophysiology as that of sepsis, DAMPs are the major activators of PRMs (12). DAMPs participate not only in sterile inflammation, but also in sepsis pathophysiology (12, 13, 20). Thus, DAMPs are regarded as an additional target for the treatment of sepsis.

Extracellular histones are DAMPs (21, 22), and they are a major cause of septic death (23). They are present in the plasma of septic patients, and they exert cytotoxic activity towards endothelial cells. Mice injected with histones display damage to the endothelium, and ultimately develop intra-alveolar hemorrhage. PTX3 binds to certain histones (24, 25), and we previously observed that extracellular histones are bound to PTX3 in plasma from septic patients (26). Although it is clear that the recognition of certain PAMPs and the activation of the subsequent innate immune response is one of the host-protective activities of PTX3 during sepsis, from the evidence discussed earlier, we hypothesized the possibility of an additional role for PTX3 in sepsis in the form of host protection against extracellular histones. Here, we investigated the detailed mechanism by which PTX3 interacted with histones and how it exerted its cytoprotective effect

against histone damage. These results suggest that PTX3 plays a major host-protective role in the response to sepsis, and thus it has potential value for sepsis treatment.

## **Results**

### **Interaction pattern between histone and PTX3**

The binding between immobilized histone H1 and PTX3 (24), as well as inhibition of the binding of immobilized PTX3 to fibroblast growth factor-2 (FGF2) by histones (25) were previously reported; however, a comprehensive analysis of the ability of PTX3 to interact with each histone has not been reported. Thus, we sought to characterize the interactions between linker and core histones and PTX3. First, we used an enzyme-linked immunosorbent assay (ELISA) to assess the interactions between immobilized histones and PTX3. We observed increased signals when full-length PTX3 was incubated with histones H1, H3, and H4, whereas we observed relatively decreased signals in the cases of histones H2A and H2B (Fig. 1A). All signals were increased in the presence of calcium ions (Fig. 1A). We further checked the interaction preference of the PTX3 domains with histones in experiments with PTX3 domain fragment proteins. The extent of interaction of the N-terminal domain of PTX3 with all the histones was greater than that of the C-terminal domain of PTX3 (Fig. 1B and fig. S1A). The oligomerization-defective PTX3 N-terminal domain, in which all of the cysteine residues were changed to serine residues, abolishes the ability of PTX3 to bind to ligands (26, 27). Compared to the signals generated by the interaction of wild-type PTX3 with all of the histones, the signals generated by the oligomerization-defective PTX3 N-terminal domain mutant were decreased (fig. S1B). These results indicate that all of the histones directly bound to PTX3, preferably through its N-terminal oligomerization domain.

We next measured apparent interaction affinities by surface plasmon resonance (SPR). We found that PTX3 had a higher affinity for histones H1, H3, and H4 than it had for histones H2A and H2B (Fig. 1C and fig. S2). There was also an increase in its affinity in the presence of calcium ions (fig. S2). Both full-length PTX3 and the PTX3 N-terminal domain showed high affinity for histones (fig. S2, A and C). In comparison, the oligomerization-deficient PTX3 N-terminal domain showed lower affinity for histones (fig. S2, B and C). Note that the affinity of the PTX3 N-terminal domain for all histones was similar to that of the full-length protein (fig. S2C). We then investigated the region(s) in the histones that were responsible for the interaction with PTX3 in experiments with synthesized peptides (20 residues in length) that covered all of the regions of histones H3 and H4 (fig. S3A and table S1). We focused on histone H3 and H4, because these histones are more cytotoxic towards endothelial cells than are the other histones (23). We analyzed the interactions between the immobilized histone fragment peptides and PTX3 by ELISA. Several peptides exhibited binding to full-length PTX3, and most of these preferentially bound to the N-terminal domain of PTX3 (fig. S3B). These results suggest there are multiple PTX3-interacting regions in histones H3 and H4.

### **Coaggregation of PTX3 with histones**

To analyze the histone-PTX3 complex from a physicochemical view, we undertook the preparation of an in-solution complex by the addition of PTX3 to a solution of histone H4. By measuring the UV-visible spectrum of the histone H4 and PTX3 mixture, we observed a dose-dependent increase in the absorbance spectrum (fig. S4). This result suggested that the spectrum pattern originated from the light-scattering of microparticles. In addition to the electron

microscopic observation of amorphous aggregates in the histone H4-PTX3 mixture (Fig. 2A), it appeared that the in-solution histone-PTX3 interaction induced coaggregates. Note that the addition of histones to serum or plasma causes a precipitate to form (28), and fibrinogen forms an aggregate with histones (29). Thus, we analyzed the formation of the histone-PTX3 coaggregate. Using the absorbance at 310 nm as a measurement of the turbidity of solutions, we analyzed the extent of coaggregation among histones and PTX3 domains. All of the histones formed coaggregates with PTX3, and higher turbidity was observed in coaggregates containing the PTX3 N-terminal domain than in aggregates containing the PTX3 C-terminal domain (Fig. 2, B and C).

### **Induction of histone-PTX3 aggregate formation by polyvalent interactions and unfolding**

To investigate the mechanisms by which histone-PTX3 aggregates formed, we set out to determine the stoichiometry of this aggregate. Various molar ratio mixtures of histone H4 and PTX3 were prepared, and, after removal of any aggregates by centrifugation, the concentrations of both proteins in the supernatant were measured (Fig. 3A). The concentration of PTX3 in the supernatant was decreased in the presence of increasing concentrations of histone H4, and was undetectable at a PTX3 monomer:histone H4 molar ratio of between 1:1 and 1:2 (Fig. 3B). These data suggest that full-length PTX3 formed aggregates with histone H4 at ratios between 1:1 and 1:2, whereas the ratios were 1:2 for the N-terminal domain and 1:1 for the C-terminal domain of PTX3. Furthermore, PTX3 was recovered from the supernatant in the case where there was an excess molar ratio of histone H4 (Fig. 3B). This suggests that, similar to the case of polyclonal antibody–antigen complex formation, histone-PTX3 aggregation is the result of a polyvalent interaction. We further investigated aggregate formation in experiments with an oligomerization-

defective PTX3 N-terminal domain. Although it was less potent than wild-type PTX3, the oligomerization-defective PTX3 N-terminal domain formed aggregates with histones (fig. S5A), and the stoichiometry of its aggregation with histone H4 was similar to that of wild-type PTX3 (fig. S5B).

To investigate other mechanisms of aggregate formation, we examined whether histone-PTX3 aggregates could be assessed by staining with thioflavin T (ThT) and 8-Anilino-1-naphthalenesulfonic acid ammonium salt (ANS), which are fluorescent dyes commonly used for the detection of aggregate formation by  $\beta$ -strand stacking or exposure of hydrophobic amino acid residues (30-32), but we did not observe any signals from histone-PTX3 aggregates (fig. S5, C and D). Thus, we next analyzed the mixture of the PTX3 N-terminal domain and histone H4 by circular dichroic (CD) spectroscopy to detect any change in the secondary structure in the histone-PTX3 complex. From the spectrum pattern of the original state of the PTX3 N-terminal domain, the presence of an  $\alpha$ -helix was suggested (Fig. 3C, upper panel), as is predicted from the amino acid sequence (6). In the histone-PTX3 mixture, the spectra were changed from the original state (Fig. 3C, the lower panel). Because these spectra did not exhibit any typical secondary structures, the result suggests that PTX3 lost its secondary structure when complexes were formed. Together, these data suggest that histone-PTX3 aggregate formation results from both the formation of a large molecular mass complex by a polyvalent interaction and a disordered aggregation caused by unfolding of the  $\alpha$ -helix of PTX3.

### **Protective effect of PTX3 against histone-mediated cytotoxicity towards endothelial cells**

The specific histone-PTX3 interaction we observed prompted us to further examine its role in modulating histone-mediated cytotoxicity towards endothelial cells (23). We found that histone-dependent cytotoxicity towards endothelial cells was attenuated by PTX3 in a dose-dependent manner (Fig. 4A). The PTX3-mediated cytoprotective effect was exhibited in the case of all of the histones (fig. S6A). PTX3 also blocked histone-dependent calcium fluxes in endothelial cells (Fig. 4B and fig. S6B). Furthermore, PTX3 substantially suppressed further calcium fluxes when it was added to culture medium after the histones had been added (Fig. 4B, right panel).

The association of histones with plasma membranes is crucial for their toxicity towards endothelial cells (33). Thus, we next checked whether PTX3 blocked the association of fluorescently labeled histones with endothelial cells. From confocal microscopic imaging, we found that, in addition to associating with the plasma membrane, histones were also internalized by the cells (fig. S6, C and D). We observed that histone aggregates formed in response to the addition of PTX3, and these precipitates increased in number in a time-dependent manner (Fig. 4C). We used flow cytometric analysis to evaluate the effect of PTX3 in blocking histone accumulation in endothelial cells. We found that histone accumulation was decreased by PTX3 in a dose-dependent manner (Fig. 4D). These results suggest that the histone-PTX3 aggregates suppress the cytotoxic effects of histones by preventing the association of histones with endothelial cells. Finally, we observed that the N-terminal domain of PTX3 exhibited a cytoprotective effect that was similar to that of full-length PTX3 (Fig. 4E).

### **In vivo cytoprotective effects of PTX3 against extracellular histones**

We further examined the protective effects of PTX3 against histone-mediated cytotoxicity in a mouse model of histone infusion. The N-terminal domain of PTX3 was administered to the mice because it was sufficient for aggregate formation (fig. S5A) and it had a cytoprotective effect against histones (fig. S7A). Administration of PTX3 substantially reduced mortality in mice infused with a high dose of histone (60 mg/kg) (Fig. 5A), which typically induces mouse lethality within 1 hour (23, 33, 34).

To investigate the host-protective effects elicited by PTX3, we performed histological examinations of mice infused with a sub-lethal dose of histones (50 mg/kg). Histone-infused mice exhibited hemorrhage in the connective tissues of the bronchiovascular bundle in the lung (Fig. 5B) and in the hilum of the lung (Fig. 5C). The extent of these hemorrhages was reduced by PTX3 (Fig. 5, B and C). Histone infusion inflicted damage on the smooth muscle fibers in the pulmonary veins (Fig. 5D), which suggested the source of the massive bleeding. Such damage was not observed in the pulmonary artery (fig. S7B). Infused histones also induced breakage of the argyrophilic fibers in the alveoli and alveolar hemorrhage (Fig. 5E). This damage was also suppressed by PTX3 (Fig. 5, D and E). Electron microscopic analysis revealed endothelial cell damage, such as cytoplasmic vacuolation, and the detachment of endothelial cells from the basal laminae in the peripheral pulmonary artery; effects that were suppressed by PTX3 (Fig. 5F). Histone infusion not only causes cytotoxicity-induced hemorrhage in vivo, it also induces thrombocytopenia (34, 35); however, we found that PTX3 did not ameliorate histone-mediated thrombocytopenia (fig. S7C). Together, the results from our in vivo experiments suggest that the reduced mortality was mainly a result of the protective effect of PTX3 against histone-mediated cytotoxicity towards endothelial cells, and that this suppressed hemorrhaging.

## **Host-protective effects of PTX3 in mouse models of sepsis**

The protective effect of the N-terminal domain of PTX3 against histone-mediated cytotoxicity *in vivo* implied that it had therapeutic potential in sepsis. Thus, we investigated its effects further in mouse models of sepsis. We found that PTX3 substantially reduced mortality in mice injected with lipopolysaccharide (LPS) (Fig. 6A). Histone H3 was detectable in the circulation 24 hours after the mice were injected with LPS, as determined by Western blotting analysis, and this increase in histone H3 concentration was suppressed by PTX3 (Fig. 6B and fig. S8). The plasma concentrations of interleukin-6 (IL-6) and vascular endothelial growth factor (VEGF) were increased in mice injected with LPS, an effect that was suppressed by PTX3 (Fig. 6C). Histological examination of the LPS-injected mice showed the recruitment of macrophages to the lung and the liver (Fig. 6D), as well as neutrophil infiltration into microvessels at alveolar walls (Fig. 6E). These effects were all substantially suppressed by PTX3 (Fig. 6F). We also observed that PTX3 resulted in a substantial reduction in mortality in mice subjected to cecal ligation and puncture (CLP), which is a widely used murine sepsis model (36), even when it was administered after the CLP operation (Fig. 6G).

## **Discussion**

Here, we report that PTX3 protects endothelial cells from extracellular histone-mediated cytotoxicity *in vitro* and *in vivo*. The administration of the N-terminal domain of PTX3 reduced mortality in mouse models of histone infusion and sepsis, which suggests that this domain is sufficient for the host-protective effect of PTX3 against septic lethality. PTX3 caused coaggregation with histones (Fig. 2). The molecular mechanisms underlying the coaggregation

involved the formation of a super-molecule by polyvalent interactions, as well as the unfolding of the  $\alpha$ -helix of PTX3 (Fig. 3) (37). That the N-terminal domain of PTX3, which is independent of the C-terminal pentraxin domain, participated in coaggregation with histones (Fig. 2, B and C) implies a correlation between the extent of coaggregation and the effect on histone-mediated cytotoxicity (Fig. 4). A previous study of PTX3-transgenic mice demonstrated that an artificially increased amount of PTX3 afforded protection against septic lethality (38). Our results suggest the possibility that, in addition to pathogen recognition in the innate immune system (3-5), PTX3 exerts a host-protective effect in sepsis by forming a tight interaction with histones such that the histone-PTX3 complexes become disordered aggregates that are prevented from interacting with the endothelial cell surface.

Compared to C-reactive protein, PTX3 is a local PRM, and its concentration in the circulation is less (39). Thus, we believe that the main physiological role of PTX3 is not protection against histone-dependent cytotoxicity, but rather, the elimination of invading microbes through opsonization, regulation of the complement cascade, and neutralization by neutrophil extracellular traps (2, 40). In turn, in the case of severe sepsis, the abundance of PTX3 is increased, and it might exert an effect as a systemic PRM. Under these conditions, PTX3 gains an additional function, namely affording protection against histone-dependent cytotoxicity. When the amount of extracellular histone protein is greater than the amount of physiological PTX3, multi-organ failure occurs (20); thus, administration of exogenous PTX3 might be a feasible treatment approach under such conditions.

The high-affinity interaction between PTX3 and various histone proteins, which was determined by ELISA and SPR analysis, appears to be a result of both multivalent interactions (fig. S2 and S3) and aggregation (Fig. 2). The unexpected observation of histone-PTX3 aggregation was mainly observed with the PTX3 N-terminal domain; however, although it had weak interactions, the C-terminal domain did form aggregates. This result raises the possibility that the short pentraxins, C-reactive protein and serum amyloid P components, which form oligomeric structures (1) and bind to histones (41, 42), may also form aggregates with histones. Because we could not detect either  $\beta$ -strand stacking or a pattern of exposure of hydrophobic residues (fig. S5, C and D), this suggests that histone-PTX3 aggregate formation is a result of polyvalent interactions and the unfolding of the  $\alpha$ -helix of PTX3 (Fig. 3). Although the co-aggregation of unstable or disordered proteins has been reported previously (43, 44), to our knowledge, this is the first report of aggregate formation induced by unfolding as a result of interaction with a heterogeneous protein.

Extracellular histones are the major mediators of death in sepsis (23). Although the detailed mechanisms of cytotoxicity are not fully known, the endosome-associated Toll-like receptor 9 (TLR9) (21) and the plasma membrane-associated TLR2 and TLR4 (22) are implicated in histone cytotoxicity in a mouse model of fatal liver injury. Although previous studies indicated that extracellular histones localized only at the plasma membrane (33, 34), we observed their partial internalization (fig. S6C), which suggests the possible participation of endosome-associated TLRs. We hypothesize that aggregation induced by PTX3 binding and disruption of the secondary structure of histones could prevent the internalization of extracellular histones. That PTX3 had protective effects against extracellular histone-dependent cytotoxicity was

further supported by the observation that histone-dependent calcium flux in endothelial cells was suppressed by PTX3 even when it was added several minutes after treatment with histones (Fig. 4B). We speculate that histone-mediated cytotoxicity is a relatively slow process, and that it can be interrupted by the potent interaction between PTX3 and histones.

In addition to our cell-based analysis, we demonstrated that PTX3 had a protective effect against extracellular histones *in vivo*. In a mouse model of histone challenge, administration of PTX3 blocked massive lung hemorrhage and vascular pathological lesion without affecting platelet function (Fig. 5). This result highlights a distinct feature of PTX3 compared with other reported protective molecules, such as anti-histone H4 antibody (23), heparin (34), C-reactive protein (33), and recombinant thrombomodulin (35). Although these molecules also bind to histones, the distinctive feature of PTX3 is its capacity to cause coaggregation, which enables PTX3 to bind rapidly and irreversibly to histones.

In our efforts to confirm the effects of administration of the N-terminal domain of PTX3 in mouse models of sepsis, we observed that PTX3 markedly rescued lethality even after the CLP operation. These findings suggest that the PTX3 N-terminal domain, which is sufficient for cytoprotection against histones, is a potential treatment for sepsis. PTX3 suppressed both pro-inflammatory signals (Fig. 6C) and the plasma concentration of histone in mice 24 hours after injection with LPS (Fig. 6B). Li *et al.* detected histone H3 in the plasma of mice 3 hours after injection with LPS (45). The discrepancy between that study and our current study may be because of the difference in the dose of LPS that was injected. Suppression of the pro-inflammatory responses to histones may be a result of the other effects of PTX3 on the innate

immune system and inflammation (2, 3). The aggregation-induced attenuation of histone cytotoxicity that we showed here may enable the rapid and permanent removal of toxic molecules, and thus may provide a new strategy for the treatment of sepsis.

## **Materials and Methods**

### **Reagents**

Recombinant histones were purchased from New England BioLabs Inc. Calf thymus histones was purchased from Roche. The anti-PTX3 mouse monoclonal antibodies PPZ-1228 (IgG2b) and horseradish peroxidase (HRP)-conjugated PPZ-1228 were generated as previously described (26). The HRP-conjugated anti-6xHis antibody (Anti-His-tag HRP-Direct) was purchased from Medical & Biological Laboratories. The anti-myc antibody (9E10) was purchased from Santa Cruz Biotechnology. The anti-histone H3 antibody (ab1791) was purchased from Abcam. The synthetic human histone H3 and H4 peptide fragments were obtained from Sigma. The peptide sequences are provided in table S1.

### **Expression and purification of PTX3 proteins**

Recombinant, non-tagged human PTX3 (rhPTX3) protein was expressed and purified as previously described (26). Recombinant, tagged human PTX3 fragments (PTX3\_Full, PTX3\_N, and PTX3\_C) were expressed and purified as previously described (26). The recombinant tagged N-terminal domain of human PTX3 (N-terminal wild-type) and its oligomerization-defective mutant, in which all of the cysteine residues were changed to serine residues (N-terminal mutant), were expressed and purified as described previously (26). Removal of endotoxin from bacterially expressed PTX3 proteins for cell-based and animal experiments was performed with

Detoxi-Gel Endotoxin Removing Columns (Thermo Fisher Scientific Inc.) according to the manufacturer's instructions.

### **Binding assays for PTX3 proteins and histone proteins**

Binding assays were performed as previously described (26). Briefly, histone or a histone peptide fragment was immobilized on a polystyrene 96-well plate. The plate was blocked with buffer containing 1% bovine serum albumin (BSA). As the primary reaction, each recombinant PTX3 protein diluted in 1% BSA buffer was added. To detect 6xHis-tagged PTX3 protein, an HRP-conjugated anti-6xHis antibody was used for the secondary reaction. To detect myc-tagged PTX3 protein, an anti-myc antibody was used for the secondary reaction, whereas a peroxidase-conjugated F(ab')<sub>2</sub> fragment goat anti-mouse IgG (H+L) was used for the third reaction. The plate was developed with soluble 3,3',5,5'-tetramethylbenzidine (TMB) reagent, and the reaction was stopped with TMB stop buffer. The absorbance was then read at 450 and 630 nm. To investigate the calcium-dependency of the interaction between PTX3 and histone proteins, 4 mM CaCl<sub>2</sub> or 4 mM each of EDTA and EGTA were added to all of the buffers.

### **SPR measurement**

All of the SPR experiments were performed with a Biacore T200. Immobilization of each recombinant human histone protein on the sensor chip CM5 was performed with an Amine Coupling Kit using a standard coupling protocol. The reaction conditions were set at 5 µl/min at 25°C with HBS-P [10 mM HEPES (pH 7.4), 150 mM NaCl, 0.05 % Tween 20] as the running buffer. All of the flow cell surfaces were activated by a 1:1 mixture of 1-Ethyl-3-[3-dimethylaminopropyl]carbodiimide hydrochloride/*N*-hydroxysuccinimide (EDC/NHS) for 7 min.

Next, each recombinant histone protein, diluted with 10 mM sodium acetate (pH 5.0), was injected for 7 min. Deactivation of excess reactive groups was achieved with a 7-min injection of ethanolamine. One flow cell, which was left uncaptured in the samples, was used as a control. The kinetic analysis was performed with a single-cycle kinetics method. With the reaction conditions set at 30  $\mu$ l/min and 25°C, five, two-fold dilutions of the analytes were injected sequentially for 2 min of association, followed by 2 min of dissociation. The highest concentration of each analyte was as follows: 1 nM for PTX3\_Full; 5 nM for PTX3\_N; 50 nM for PTX\_C; 5 nM for the N-terminal wild-type; and 50 nM for the N-terminal mutant. Regeneration of the surface was achieved by an injection of 0.1 % SDS for 7 min. To investigate the calcium-dependency of the interaction, 3 mM CaCl<sub>2</sub> or 3 mM each of EDTA and EGTA were added to the buffer during the kinetic analysis. The kinetics were calculated with Biacore T200 evaluation software.

### **Turbidity measurement**

Turbidity measurement was performed with a NanoDrop spectrophotometer (Thermo Scientific). Before the turbidity measurements, samples were dialyzed with Tris-buffered saline (TBS) containing 4 mM CaCl<sub>2</sub>.

### **Transmission electron microscopy**

Transmission electron microscopy analysis was performed as previously described (46). Briefly, the histone-PTX3 mixtures were mixed and then fixed in a 1% OsO<sub>4</sub> solution for 1 hour. A drop of the mixture was placed on a grid provided with a supporting collodion film. Photographs were taken under transmission electron microscopy (S700; Hitachi).

### **Fluorescent probe-based aggregation assay**

All of the fluorescence measurements were performed with Fusion universal microplate reader (PerkinElmer). To detect aggregation caused by  $\beta$ -sheet stacking, 5  $\mu$ M (final concentration) thioflavin T (ThT, Sigma) was added to the samples. To detect hydrophobicity-mediated aggregation, 1  $\mu$ M (final concentration) 8-Anilino-1-naphthalenesulfonic acid ammonium salt (ANS, Sigma) was added to the samples. The excitation and emission maximums for each measurement were set to 425 and 485 nm for ThT and 330 and 485 nm for ANS, respectively.

### **CD analysis**

CD spectra were recorded on a J-820 spectropolarimeter (JASCO). Measurements were performed in TBS containing 4 mM  $\text{CaCl}_2$  at 25°C with a quartz cuvette with a path length of 0.1 cm (GL Sciences Inc.). All of the measurements were performed with the indicated concentrations of TBS containing 4 mM  $\text{CaCl}_2$ . Samples were scanned five times at 20 nm/min with a bandwidth of 0.1 nm and a response time of 1 s over the wavelength range 190 to 260 nm. The data were averaged and the spectrum of the buffer sample was subtracted.

### **Cytotoxicity assays**

Human umbilical vein endothelial cells (HUVECs) were cultured in EGM2 medium (Clonetics), and were used for experiments within the first 6 passages. For the cytotoxicity assay, cultured HUVECs were washed with phosphate-buffered saline (PBS) and incubated with various histones mixed with or without PTX3 in Opti-MEM medium at 37°C for 1 hour, and then were stained by adding propidium iodide (PI, 10  $\mu$ g/ml, Sigma) for 5 min at 37°C. The cells were

washed with PBS and detached with PBS, 0.2 % Pluronic F-68, 1 mM EDTA, and then were subjected to flow cytometric analysis.

### **Ca<sup>2+</sup> signal imaging**

The human umbilical vein cell line EA.hy926 cells (ATCC) were cultured on glass base dishes (ASAHI GLASS CO., LTD) in DMEM supplemented with 10% fetal bovine serum. Cells were pre-loaded with Fluo 4-AM (Dojindo) according to the manufacturer's instructions. After washing with PBS, cells were incubated with Hank's Balanced Salt Solution (HBSS) containing 3 mM CaCl<sub>2</sub>. Cells were treated with histones in the absence or presence of PTX3 in HBSS containing 3 mM CaCl<sub>2</sub>, and then fluorescence images were acquired at 5-s intervals by confocal laser scanning microscopy (FV-1000; Olympus). The acquired images were analyzed with MetaMorph imaging software (v6.2, Molecular Devices).

### **Analysis of histone localization with endothelial cells**

Calf thymus histones or BSA were labeled with an Alexa Fluor 488 protein-labeling kit (Invitrogen) according to the manufacturer's instructions. EA.hy926 cells were cultured on glass base dishes. Cells were pre-loaded with CellTracker Orange Fluorescent Probe (Takara Bio) according to the manufacturer's instructions. After washing with PBS, cells were incubated with HBSS containing 3 mM CaCl<sub>2</sub>. Cells were treated with Alexa Fluor-conjugated histones with or without PTX3 in HBSS containing 3 mM CaCl<sub>2</sub>. Cells were washed with PBS, fixed with 4% paraformaldehyde in PBS for 10 min at room temperature, washed with PBS, and incubated with HBSS containing 3 mM CaCl<sub>2</sub>. Fluorescence images were captured by confocal laser scanning microscopy (FV-1000; Olympus).

## **Animal experiments**

We used male 6- to 12- week-old C57BL/6 mice for the animal experiments. All animal studies were approved by the Institutional Animal Care and Use Committees at the University of Tokyo. For the histone-infusion model, mice were intravenously injected with calf thymus histones at 60 mg/kg or 50 mg/kg body weight. Mice were treated with or without PTX3 (N-terminal wild-type, 12 mg/kg body weight) by intraperitoneal injection just before the histones were infused. Lung samples were fixed in formalin, embedded, sectioned, stained with hematoxylin and eosin, and subjected to Elastica van Gieson staining and Reticulin staining. Paraformaldehyde fixation was used for electron microscopic observation. For the LPS-induced endotoxemia model, mice were injected with LPS (Lot. 090M4030, Sigma, 16 mg/kg body weight). Mice were treated with or without PTX3 (N-terminal wild-type, 5 mg/kg body weight) by intraperitoneal injection 2 hours before they were challenged with LPS. Measurement of the concentrations of IL-6 and VEGF in the plasma of LPS-injected mice was performed as previously described (47). The liver and lungs were removed 24 hours after LPS injection, fixed in 10% buffered formalin, and embedded in paraffin. To identify neutrophils, histological slides were deparaffinized and rehydrated. The slides were stained for naphthol AS-D chloroacetate esterase according to the manufacturer's instructions (Naphthol AS-D Chloroacetate Esterase Kit; Sigma-Aldrich) and were counterstained with hematoxylin. The neutrophils within these areas, identified by red cytoplasmic staining and typical polymorphonuclear morphology, were then counted. With imaging software (NIS- Elements D; Nikon Inc.), at least  $25 \times 10^{-2} \text{ mm}^2$  or more areas were selected randomly and averaged. The results from each count were expressed as the neutrophil number /  $5 \times 10^{-2} \text{ mm}^2$  for the section. For immunohistochemistry, the specimens were stained

with an anti-mouse F4/80 rat monoclonal antibody (BMA Biomedicals) as previously described (48). Stained cells were counted in ten randomly chosen 6.25 mm<sup>2</sup> squares with an eyepiece (Olympus WHK 10x/20L). For CLP-induced sepsis model, the CLP procedure was performed as described previously (49). Mice were treated with gentamicin (5 mg/kg body weight) and PTX3 (N-terminal wild-type, 5 mg/kg body weight) or gentamicin alone by intraperitoneal injection 4 hours after the CLP procedure was performed.

## Statistics

Results are mean  $\pm$  SD unless otherwise stated. We analyzed calcium imaging data with Bonferroni post tests. We analyzed mouse survival with the log-rank test.  $P < 0.05$  was considered statistically significant. Other statistical analyses were performed with  $P$  values calculated by the Student's  $t$  test.

## Supplementary Materials

Fig. S1. Analysis of histone-PTX3 interactions by ELISA.

Fig. S2. Analysis of histone-PTX3 interactions by SPR.

Fig. S3. Analysis of the interaction between histone peptides and PTX3.

Fig. S4. UV-visible spectrum of a histone-PTX3 mixture.

Fig. S5. Assessments of histone-PTX3 aggregation.

Fig. S6. PTX3-mediated protection against cytotoxicity that is caused by the association of histones with the endothelium.

Fig. S7. Effects of PTX3 in histone-infused mice.

Fig. S8. Time-course analysis of plasma histone H3 concentrations in LPS-treated mice.

Table S1. List of the histone H3 and H4 fragment peptides.

## References and Notes

1. C. Garlanda, B. Bottazzi, A. Bastone, A. Mantovani, Pentraxins at the crossroads between innate immunity, inflammation, matrix deposition, and female fertility. *Annu Rev Immunol* **23**, 337-366 (2005).
2. B. Bottazzi, A. Doni, C. Garlanda, A. Mantovani, An Integrated View of Humoral Innate Immunity: Pentraxins as a Paradigm. *Annual Review of Immunology* **28**, 157-183 (2010).
3. A. Mantovani, C. Garlanda, A. Doni, B. Bottazzi, Pentraxins in innate immunity: from C-reactive protein to the long pentraxin PTX3. *J Clin Immunol* **28**, 1-13 (2008).

4. A. Doni, C. Garlanda, B. Bottazzi, S. Meri, P. Garred, A. Mantovani, Interactions of the humoral pattern recognition molecule PTX3 with the complement system. *Immunobiology* **217**, 1122-1128 (2012).
5. A. Mantovani, S. Valentino, S. Gentile, A. Inforzato, B. Bottazzi, C. Garlanda, The long pentraxin PTX3: a paradigm for humoral pattern recognition molecules. *Ann N Y Acad Sci*, (2013).
6. M. Presta, M. Camozzi, G. Salvatori, M. Rusnati, Role of the soluble pattern recognition receptor PTX3 in vascular biology. *J Cell Mol Med* **11**, 723-738 (2007).
7. A. Inforzato, S. Jaillon, F. Moalli, E. Barbati, E. Bonavita, B. Bottazzi, A. Mantovani, C. Garlanda, The long pentraxin PTX3 at the crossroads between innate immunity and tissue remodelling. *Tissue antigens* **77**, 271-282 (2011).
8. A. Inforzato, P. C. Reading, E. Barbati, B. Bottazzi, C. Garlanda, A. Mantovani, The "sweet" side of a long pentraxin: how glycosylation affects PTX3 functions in innate immunity and inflammation. *Front Immunol* **3**, 407 (2012).
9. L. Deban, B. Bottazzi, C. Garlanda, Y. M. de la Torre, A. Mantovani, Pentraxins: multifunctional proteins at the interface of innate immunity and inflammation. *BioFactors* **35**, 138-145 (2009).
10. P. Cieslik, A. Hrycek, Long pentraxin 3 (PTX3) in the light of its structure, mechanism of action and clinical implications. *Autoimmunity* **45**, 119-128 (2012).
11. G. S. Martin, D. M. Mannino, S. Eaton, M. Moss, The epidemiology of sepsis in the United States from 1979 through 2000. *N Engl J Med* **348**, 1546-1554 (2003).
12. A. Castellheim, O. L. Brekke, T. Espevik, M. Harboe, T. E. Mollnes, Innate immune responses to danger signals in systemic inflammatory response syndrome and sepsis. *Scand J Immunol* **69**, 479-491 (2009).
13. M. Jedynek, A. Siemiątkowski, K. Rygasiewicz, Molecular basics of sepsis development. *Anaesthesiol Intensive Ther* **44**, 221-225 (2012).
14. M. Aziz, A. Jacob, W. L. Yang, A. Matsuda, P. Wang, Current trends in inflammatory and immunomodulatory mediators in sepsis. *J Leukoc Biol* **93**, 329-342 (2013).
15. B. Muller, G. Peri, A. Doni, V. Torri, R. Landmann, B. Bottazzi, A. Mantovani, Circulating levels of the long pentraxin PTX3 correlate with severity of infection in critically ill patients. *Crit Care Med* **29**, 1404-1407 (2001).
16. T. Mauri, G. Bellani, N. Patroniti, A. Coppadoro, G. Peri, I. Cuccovillo, M. Cugno, G. Iapichino, L. Gattinoni, A. Pesenti, A. Mantovani, Persisting high levels of plasma pentraxin 3 over the first days after severe sepsis and septic shock onset are associated with mortality. *Intensive Care Med* **36**, 621-629 (2010).
17. R. Uusitalo-Seppälä, R. Huttunen, J. Aittoniemi, P. Koskinen, A. Leino, T. Vahlberg, E. M. Rintala, Pentraxin 3 (PTX3) is associated with severe sepsis and fatal disease in emergency room patients with suspected infection: a prospective cohort study. *PLoS One* **8**, e53661 (2013).
18. M. E. Bianchi, DAMPs, PAMPs and alarmins: all we need to know about danger. *J Leukoc Biol* **81**, 1-5 (2007).
19. K. Newton, V. M. Dixit, Signaling in innate immunity and inflammation. *Cold Spring Harb Perspect Biol* **4**, (2012).
20. S. Denk, M. Perl, M. Huber-Lang, Damage- and pathogen-associated molecular patterns and alarmins: keys to sepsis? *Eur Surg Res* **48**, 171-179 (2012).

21. H. Huang, J. Evankovich, W. Yan, G. Nace, L. Zhang, M. Ross, X. Liao, T. Billiar, J. Xu, C. T. Esmon, A. Tsung, Endogenous histones function as alarmins in sterile inflammatory liver injury through Toll-like receptor 9 in mice. *Hepatology* **54**, 999-1008 (2011).
22. J. Xu, X. Zhang, M. Monestier, N. L. Esmon, C. T. Esmon, Extracellular histones are mediators of death through TLR2 and TLR4 in mouse fatal liver injury. *J Immunol* **187**, 2626-2631 (2011).
23. J. Xu, X. Zhang, R. Pelayo, M. Monestier, C. T. Ammollo, F. Semeraro, F. B. Taylor, N. L. Esmon, F. Lupu, C. T. Esmon, Extracellular histones are major mediators of death in sepsis. *Nat Med* **15**, 1318-1321 (2009).
24. B. Bottazzi, V. Vouret-Craviari, A. Bastone, L. De Gioia, C. Matteucci, G. Peri, F. Spreafico, M. Pausa, C. D'Ettoire, E. Gianazza, A. Tagliabue, M. Salmona, F. Tedesco, M. Introna, A. Mantovani, Multimer formation and ligand recognition by the long pentraxin PTX3. Similarities and differences with the short pentraxins C-reactive protein and serum amyloid P component. *J Biol Chem* **272**, 32817-32823 (1997).
25. M. Rusnati, M. Camozzi, E. Moroni, B. Bottazzi, G. Peri, S. Indraccolo, A. Amadori, A. Mantovani, M. Presta, Selective recognition of fibroblast growth factor-2 by the long pentraxin PTX3 inhibits angiogenesis. *Blood* **104**, 92-99 (2004).
26. K. Daigo, N. Yamaguchi, T. Kawamura, K. Matsubara, S. Jiang, R. Ohashi, Y. Sudou, T. Kodama, M. Naito, K. Inoue, T. Hamakubo, The proteomic profile of circulating pentraxin 3 (PTX3) complex in sepsis demonstrates the interaction with azurocidin 1 and other components of neutrophil extracellular traps. *Mol Cell Proteomics* **11**, M111 015073 (2012).
27. A. Inforzato, C. Baldock, T. A. Jowitt, D. F. Holmes, R. Lindstedt, M. Marcellini, V. Riviaccio, D. C. Briggs, K. E. Kadler, A. Verdoliva, B. Bottazzi, A. Mantovani, G. Salvatori, A. J. Day, The angiogenic inhibitor long pentraxin PTX3 forms an asymmetric octamer with two binding sites for FGF2. *The Journal of biological chemistry* **285**, 17681-17692 (2010).
28. A. D. Pemberton, J. K. Brown, N. F. Inglis, Proteomic identification of interactions between histones and plasma proteins: Implications for cytoprotection. *Proteomics* **10**, 1484-1493 (2010).
29. S. L. Gonias, J. J. Pasqua, C. Greenberg, S. V. Pizzo, Precipitation of fibrinogen, fibrinogen degradation products and fibrin monomer by histone H3. *Thromb Res* **39**, 97-116 (1985).
30. M. Biancalana, S. Koide, Molecular mechanism of Thioflavin-T binding to amyloid fibrils. *Biochim Biophys Acta* **1804**, 1405-1412 (2010).
31. J. R. Daban, M. D. Guasch, Exposed hydrophobic regions in histone oligomers studied by fluorescence. *Biochim Biophys Acta* **625**, 237-247 (1980).
32. R. Khurana, C. Coleman, C. Ionescu-Zanetti, S. A. Carter, V. Krishna, R. K. Grover, R. Roy, S. Singh, Mechanism of thioflavin T binding to amyloid fibrils. *J Struct Biol* **151**, 229-238 (2005).
33. S. T. Abrams, N. Zhang, C. Dart, S. S. Wang, J. Thachil, Y. Guan, G. Wang, C. H. Toh, Human CRP Defends against the Toxicity of Circulating Histones. *J Immunol* **191**, 2495-2502 (2013).
34. T. A. Fuchs, A. A. Bhandari, D. D. Wagner, Histones induce rapid and profound thrombocytopenia in mice. *Blood* **118**, 3708-3714 (2011).

35. M. Nakahara, T. Ito, K. Kawahara, M. Yamamoto, T. Nagasato, B. Shrestha, S. Yamada, T. Miyauchi, K. Higuchi, T. Takenaka, T. Yasuda, A. Matsunaga, Y. Kakihana, T. Hashiguchi, Y. Kanmura, I. Maruyama, Recombinant Thrombomodulin Protects Mice against Histone-Induced Lethal Thromboembolism. *PLoS One* **8**, e75961 (2013).
36. L. Dejager, I. Pinheiro, E. Dejonckheere, C. Libert, Cecal ligation and puncture: the gold standard model for polymicrobial sepsis? *Trends Microbiol* **19**, 198-208 (2011).
37. C. M. Dobson, Protein folding and misfolding. *Nature* **426**, 884-890 (2003).
38. A. A. Dias, A. R. Goodman, J. L. Dos Santos, R. N. Gomes, A. Altmeyer, P. T. Bozza, M. F. Horta, J. Vilcek, L. F. Reis, TSG-14 transgenic mice have improved survival to endotoxemia and to CLP-induced sepsis. *J Leukoc Biol* **69**, 928-936 (2001).
39. K. Daigo, A. Mantovani, B. Bottazzi, The yin-yang of long pentraxin PTX3 in inflammation and immunity. *Immunol Lett* **161**, 38-43 (2014).
40. K. Daigo, T. Hamakubo, Host-protective effect of circulating pentraxin 3 (PTX3) and complex formation with neutrophil extracellular traps. *Front Immunol* **3**, 378 (2012).
41. T. W. Du Clos, L. T. Zlock, R. L. Rubin, Analysis of the binding of C-reactive protein to histones and chromatin. *J Immunol* **141**, 4266-4270 (1988).
42. P. S. Hicks, L. Saunero-Nava, T. W. Du Clos, C. Mold, Serum amyloid P component binds to histones and activates the classical complement pathway. *J Immunol* **149**, 3689-3694 (1992).
43. H. Olzscha, S. M. Schermann, A. C. Woerner, S. Pinkert, M. H. Hecht, G. G. Tartaglia, M. Vendruscolo, M. Hayer-Hartl, F. U. Hartl, R. M. Vabulas, Amyloid-like aggregates sequester numerous metastable proteins with essential cellular functions. *Cell* **144**, 67-78 (2011).
44. J. Xu, J. Reumers, J. R. Couceiro, F. De Smet, R. Gallardo, S. Rudyak, A. Cornelis, J. Rozenski, A. Zwolinska, J. C. Marine, D. Lambrechts, Y. A. Suh, F. Rousseau, J. Schymkowitz, Gain of function of mutant p53 by coaggregation with multiple tumor suppressors. *Nat Chem Biol* **7**, 285-295 (2011).
45. Y. Li, B. Liu, E. Y. Fukudome, J. Lu, W. Chong, G. Jin, Z. Liu, G. C. Velmahos, M. Demoya, D. R. King, H. B. Alam, Identification of citrullinated histone H3 as a potential serum protein biomarker in a lethal model of lipopolysaccharide-induced shock. *Surgery* **150**, 442-451 (2011).
46. M. Naito, E. Wisse, Filtration effect of endothelial fenestrations on chylomicron transport in neonatal rat liver sinusoids. *Cell Tissue Res* **190**, 371-382 (1978).
47. T. Minami, K. Yano, M. Miura, M. Kobayashi, J. Suehiro, P. C. Reid, T. Hamakubo, S. Ryeom, W. C. Aird, T. Kodama, The Down syndrome critical region gene 1 short variant promoters direct vascular bed-specific gene expression during inflammation in mice. *J Clin Invest* **119**, 2257-2270 (2009).
48. T. Yamamoto, C. Kaizu, T. Kawasaki, G. Hasegawa, H. Umezumi, R. Ohashi, J. Sakurada, S. Jiang, L. Shultz, M. Naito, Macrophage colony-stimulating factor is indispensable for repopulation and differentiation of Kupffer cells but not for splenic red pulp macrophages in osteopetrotic (op/op) mice after macrophage depletion. *Cell Tissue Res* **332**, 245-256 (2008).
49. D. Rittirsch, M. S. Huber-Lang, M. A. Flierl, P. A. Ward, Immunodesign of experimental sepsis by cecal ligation and puncture. *Nat Protoc* **4**, 31-36 (2009).

**Acknowledgments:** We thank C. Saruta and K. Suga for their excellent technical assistance. We thank A. Mantovani (Istituto Clinico Humanitas IRCCS and University of Milan) for critical reading and valuable suggestions about the manuscript. We also thank K. Boru of Pacific Edit for review of the manuscript. **Funding:** This work was supported by Japan Grants-in-Aid for Scientific Research 20221010, 21590397, and 25220205 from the Ministry of Education, Culture, Sports, Science and Technology, collaborative research of the University of Tokyo and JSR Corporation, and Young Scientists Development Program, Research Center for Advanced Science and Technology at University of Tokyo (funded by FUJIFILM Corporation). **Author contributions:** K.D. and T.H. conceived of the study idea and designed the experiments; K.D. and R.F. expressed and purified recombinant PTX3 proteins; N.Y. and K.I. provided hypothesis and ideas on cytotoxic assay; K.D. performed ELISA and cytotoxic assays; K.D., R.F., and T.M. designed and conducted mouse experiments; R.O., K.M., S.J., and M. Naito designed, conducted, and analyzed data from histological examinations and electron microscopic analysis; K.D. conducted SPR analysis; K.T. provided ideas on the aggregation assay; K.D., M. Nakakido, and K.T. designed and conducted aggregation assays and CD spectra measurements; K.D., K.T., and T.H. analyzed the data; and K.D. and T.H. wrote the manuscript. **Competing interests:** K.D., K.I., K.T., and T.H. are co-inventors of a patent on “Agent for treating or preventing systemic inflammatory response syndrome” (WO2013191280 A1). The other authors declare that they have no competing interests.

**Fig. 1. Binding pattern and affinity of PTX3 and histones.** (A) The extent of binding of recombinant, non-tagged human PTX3 (rhPTX3) to the indicated histone proteins in the presence ( $\text{Ca}^{2+}$ ) and absence (EDTA/EGTA) of calcium was measured by ELISA as described in the Materials and Methods. The HRP-conjugated anti-PTX3 monoclonal antibody PPZ-1228 was used for detection. Data are from three independent experiments performed in duplicate. (B) The extent of binding of the indicated recombinant tagged human PTX3 fragments to histone H4 in the presence (left) and absence (right) of calcium was measured by ELISA. An HRP-conjugated anti-myc antibody was used for detection. Data are from three independent experiments performed in duplicate. (C) Binding sensorgrams and calculated affinities of the interaction between histone H4 and the indicated recombinant tagged human PTX3 fragments in the presence ( $\text{Ca}^{2+}$ ) and absence (EDTA/EGTA) of calcium as determined by SPR measurements. SPR sensorgrams are representative of two or three independent experiments. The calculated

affinities shown below the graphs are from two or three independent experiments. The extents of binding and affinities of the PTX3 fragments and other histones can be found in figs. S1 and S2.

**Fig. 2. Histone-PTX3 binding causes aggregate formation.** (A) Electron microscopic image of the aggregates formed in a mixture of histone H4 (0.5 mg/ml) and the N-terminal domain of wild-type PTX3 (0.17 mg/ml). Scale bar: 0.2  $\mu$ m. Image is representative of two independent experiments. (B) The indicated recombinant histone proteins (50  $\mu$ g/ml) were mixed with each of the indicated PTX3 fragments (30  $\mu$ g/ml), and the turbidity of the resulting mixtures was measured as described in the Materials and Methods. Data are means  $\pm$  SD from two independent experiments. (C) Calf thymus histones (Histones, 50  $\mu$ g/ml) were mixed with a range of concentrations of the indicated PTX3 fragments, and the turbidity of the resulting mixtures was measured as described earlier. Data are means  $\pm$  SD from two independent experiments.

**Fig. 3. The molecular mechanisms of histone-PTX3 aggregate formation.** (A) Method used to determine the stoichiometry of aggregate formation. (B) Determination of the stoichiometry of histone-PTX3 aggregates. The indicated PTX3 fragments (50  $\mu$ g/ml) were mixed with the indicated molar ratios of histone H4 protein, aggregates were removed by centrifugation, and the residual PTX3 and histone H4 proteins in the supernatant were resolved by SDS-PAGE. The gels were stained with CYPRO Ruby. Images are representative of two independent experiments. (C) Top: The CD spectra of PTX3 N-terminal wild-type (25  $\mu$ g/ml), PTX3 N-terminal mutant (25  $\mu$ g/ml), and histone H4 (5  $\mu$ g/ml). Bottom: The CD spectra of mixtures of the indicated PTX3 proteins and histone H4. To ensure adequate measurements, concentrations of PTX3 and histone

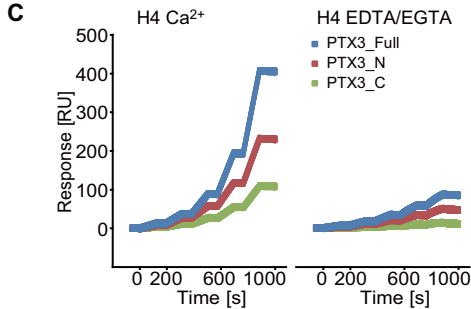
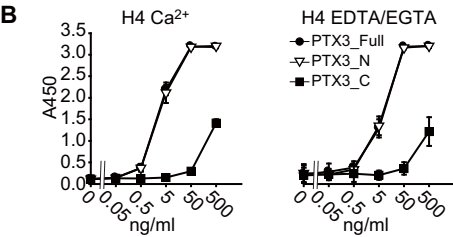
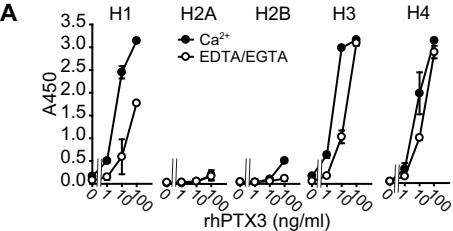
H4 that resulted in no aggregation were used (fig. S5E). Before all experiments, samples were dialyzed with TBS containing 4 mM CaCl<sub>2</sub>. Spectra are representative of two independent experiments.

**Fig. 4. PTX3-mediated protection of endothelial cells from cytotoxicity caused by extracellular histones.** (A) The ability of PTX3 to protect HUVECs from the cytotoxic effects of the indicated concentrations of calf thymus histones (Histones) was assessed by staining the cells with propidium iodide (PI) and determining the mean fluorescence intensity (MFI) of PI staining. Data are means  $\pm$  SD from three independent experiments. (B) The ability of PTX3 to suppress histone-mediated calcium flux in EA.hy926 cells was determined by measuring a calcium indicator dye in loaded cells. The fluorescence images were taken at five-second intervals with a microscope, and the numbers of cells that exhibited increased fluorescence intensity within groups of 25 cells in each set of 6 frames were counted. Left: Histone (Control) or a histone-PTX3 mixture (PTX3\_Full) was added. Right: Histone was added at 0 s, and then either medium (Control) or PTX3 (PTX3\_Full) was subsequently added at 180 s. Data are means  $\pm$  SD from three independent experiments. \* $P$  < 0.05, \*\* $P$  < 0.01, and \*\*\* $P$  < 0.001 compared to control. (C) EA.hy926 endothelial cells stained with CellTracker Orange were incubated for the indicated times with Alexa Fluor 488–labeled histones (40  $\mu$ g/ml) alone or in the presence of full-length PTX3 protein (20  $\mu$ g/ml). The localization of the histones in relation to the endothelial cells was observed by confocal microscopy. Scale bar: 100  $\mu$ m. Images are representative of three independent experiments. (D) EA.hy926 cells were incubated with Alexa Fluor 488–conjugated histones or BSA in the presence of the indicated concentrations of full-length PTX3 protein. Cells were then analyzed by flow cytometry to measure the MFI of bound

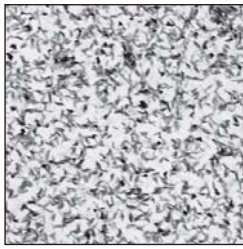
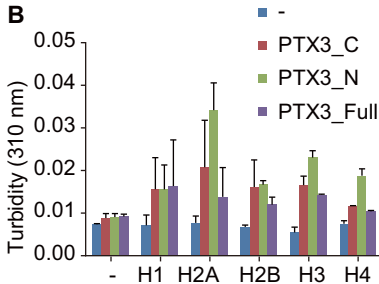
fluorescently labeled protein. Data are means  $\pm$  SD from three independent experiments. (E) HUVECs were treated with calf thymus histones (Histones, 100  $\mu$ g/ml) in the presence or absence of the indicated human PTX3 fragments (40  $\mu$ g/ml). Cells were then incubated with PI, and extent of PI staining was measured by flow cytometric analysis as described earlier. Data are representative of three independent experiments.

**Fig. 5. Analysis of the protective effects of the N-terminal domain of PTX3 against histone infusion in mice.** Histone-infused mice were treated with the PTX3 N-terminal domain (N-terminal wild-type) or control buffer (Control). (A) Survival rates of mice intravenously injected with histones (60 mg/kg) over time. Data are from five mice for each treatment. (B to F) PTX3-mediated suppression of hemorrhage and other damage in the lungs. Lungs removed from mice 120 min after they were infused with sub-lethal doses of histones (50 mg/kg) were stained by (B and C) H&E staining, (D) (top) H&E staining, (bottom) Elastica van Gieson staining, (E) Reticulin staining, or (F) were analyzed by electron microscopy. Histone-induced hemorrhages were observed in (B) the bronchovascular bundle (arrows) and (C) hilum of the lung (arrows). (D) Histone-induced disruption of smooth muscle fibers and desquamation of endothelium and elastic fiber were observed in pulmonary veins (arrows). (E) Histone-induced rupture of the alveolar walls was observed (arrows). (F) Histone-induced cytotoxicity of endothelial cells was observed by electron microscopy. The areas indicated by boxes are enlarged and are shown below. Hemorrhaging and other damage in the mice were suppressed by the administration of the N-terminal domain of PTX3. Scale bars: 500  $\mu$ m (B and C), 50  $\mu$ m (D and E), and 25  $\mu$ m (F). Data in (B) to (F) are representative of three mice for each treatment.

**Fig. 6. Analysis of the host-protective effects of the N-terminal domain of PTX3 against sepsis in mouse models.** (A to F) Mice were treated with LPS and then were treated with either the N-terminal domain of PTX3 (N-terminal wild-type) or control buffer (Control). (A) Survival rates of mice intravenously injected with LPS over time. Data are from 16 mice for each treatment. (B) The presence of plasma histone H3 protein was detected 24 hours after injection with LPS. Data are from five mice for each treatment. Analysis of the time course is shown in fig. S8. (C) The plasma concentrations of IL-6 and VEGF in the LPS-injected mice at the indicated times were measured by ELISA. Data are means  $\pm$  SEM from five mice for each treatment.  $*P < 0.05$ . (D) Macrophage recruitment into the lung (top) and liver (bottom) 24 hours after LPS injection was determined by immunostaining with an anti-F4/80 antibody. Scale bar: 50  $\mu$ m. Images are representative of four mice for each treatment. (E) Neutrophil recruitment into the lung 24 hours after LPS injection was determined by esterase staining. Scale bar: 50  $\mu$ m. Images are representative of five mice for each treatment. (F) Numbers of macrophages in the lung and the liver, and of neutrophils in the lung.  $*P < 0.05$ ,  $**P < 0.005$ . Data are means  $\pm$  SD from four or five mice for each treatment. (G) Survival rates of mice subjected to CLP. Mice were treated with gentamicin alone (Control) or in the presence of the N-terminal domain of PTX3 (N-terminal wild-type). Data are from the indicated numbers of mice for each treatment.



$K_D$ (M)	H4 $\text{Ca}^{2+}$	H4 EDTA/EGTA
PTX3_Full	$1.07 \pm 1.28 \times 10^{-11}$	$3.44 \pm 0.29 \times 10^{-11}$
PTX3_N	$3.35 \pm 0.53 \times 10^{-10}$	$3.46 \pm 0.14 \times 10^{-10}$
PTX3_C	$1.04 \pm 1.69 \times 10^{-9}$	$3.22 \pm 5.45 \times 10^{-7}$

**A****B****C**